Energy Engineering

Tech Science Press

Doi:10.32604/ee.2025.071463

ARTICLE

Performance Optimization of an Integrated Full-Capacity Domestic Hot Water Supply System for Hotel Applications

Lanyue Liu[1], Chunzhi Zhang[1,*] and Zhongyi Yu[2]

[1]School of Urban Construction, Wuhan University of Science and Technology, Wuhan, 430065, China
[2]CITIC Architectural Design and Research Institute Co., Ltd., Wuhan, 430014, China

*Corresponding Author: Chunzhi Zhang. Email: zhangchunzhi@wust.edu.cn

Received: 06 August 2025; Accepted: 04 November 2025; Published: 27 April 2026

ABSTRACT: This study develops an optimized integrated system for full-capacity hot water supply in hotels by combining solar thermal energy and air-source heat pumps. Using a hotel in Wuhan as a case study, a four-season × four-occupancy multidimensional working-condition matrix was established. Dynamic simulation and multi-objective optimization were performed on TRNSYS-TRNOPT, with the cost-benefit ratio (CBR) as the core evaluation metric. Key parameters—including collector area, tilt and azimuth angles, heat pump capacity, and storage tank volume—were jointly optimized. Model calibration against measured data yielded a deviation of less than 8%. The results demonstrate that the optimized system can achieve 60.8% energy savings and reduce annual carbon emissions by 132.8 t. The best-performing case (Case 1-1) achieved a payback period of 4.1 years, presenting a feasible pathway for decarbonizing buildings with high hot water demand. This research confirms the technical and economic viability of solar–heat pump systems for hotel applications, providing strong support for the achievement of China's "Dual Carbon" targets in public buildings.

KEYWORDS: Domestic hot water; solar energy; air-source heat pump (ASHP); full-load supply; performance optimization; TRNSYS simulation

1 Introduction

The International Energy Agency (IEA) projects that China's total CO_2 emissions will reach approximately 12.6 billion tons in 2023, representing a 4.7% annual increase and accounting for 33.7% of global emissions. Notably, 88.8% of these emissions originate from direct energy combustion, which itself shows a 5.2% annual growth rate. The construction industry, as the largest contributor to global energy consumption and carbon emissions, accounts for 36% of worldwide end-use energy consumption and 39% of total carbon emissions [1]. During the operational phase of buildings, carbon emissions contribute about 22% of the total, with domestic hot water (DHW) systems responsible for approximately 15% [2].

As high-energy-consuming public buildings, hotels exemplify the challenges in achieving a low-carbon energy transition in China's construction sector. Their hot water supply systems face intense instantaneous load fluctuations and concentrated thermal demands. However, empirical evidence reveals persistent structural issues: heavy dependence on fossil fuels and slow technological progress. Survey data indicate that most hotel hot water systems rely on single heat sources, particularly boilers, while only a small proportion adopt hybrid systems such as solar-assisted collectors or combined solar–heat pump/boiler configurations. This

Copyright © 2026 The Authors. Published by Tech Science Press.
This work is licensed under a Creative Commons Attribution 4.0 International License, which permits unrestricted use, distribution, and reproduction in any medium, provided the original work is properly cited.

fossil fuel–dominated structure results in consistently high carbon intensity, which directly conflicts with China's "Dual Carbon" strategy.

A comparative analysis of mainstream DHW supply systems (Table 1) shows that although traditional gas boilers require lower initial investment, their low efficiency and high fossil fuel consumption are major sources of carbon emissions. By contrast, air-source heat pumps (ASHPs) offer higher efficiency and moderate investment costs but remain sensitive to climatic conditions. The "solar + heat pump" hybrid system emerges as the most technically and economically advantageous option, capable of significantly reducing both energy use and carbon emissions. Nonetheless, it demands higher upfront investment and specific site conditions.

Table 1: Comparison of mainstream domestic hot water supply systems

System type	Efficiency (COP)	Initial investment	Applicable scenarios	Primary energy source
Boiler	0.8~0.9	Low	Regions with low natural gas prices/Backup heat source	Gas/Electricity
Air Source Heat Pump (ASHP)	3.0~4.5	Medium	More suitable for temperate climates or regions with mild winters	Electricity (partially from renewables)
Solar Collector + Heat Pump	4.0~6.0	High	Regions with high solar radiation	Solar (primary) + Electricity (auxiliary)
PCM Storage + Heat Pump	4.5~5.5	High	Regions with significant electricity price differentials (peak/off-peak)	Electricity (primary) + Thermal storage media
PVT + Heat Pump	4.0~6.0	Very high	Space-constrained, high solar radiation regions where simultaneous heat/electricity demand exists	Solar (primary) + Electricity (auxiliary/complementary)

The IEA identifies the building sector's energy transition as a critical pathway toward global carbon neutrality, highlighting integrated solar–air-source heat pump systems as a promising solution [3]. Wang et al. [4] further confirm the superior efficiency and emission-reduction potential of solar-assisted heat pumps, particularly in high water-demand buildings such as hotels. Bhadra and Mwesigye [5] investigated solar-assisted ASHPs for DHW in cold climates. At solar radiation ≥ 300 W/m^2 and outdoor temperature ≥ −25°C, coupling with solar air collectors improved the COP by 18.2%, reduced annual energy consumption by 20%, and shortened operation time to 429 h; air recirculation further raised COP by 24.2%. Ma et al. [6] simulated a solar-ASHP system via TRNSYS. Its time-temperature difference strategy met DHW demand and saved energy (theoretical 50°C supply, occasionally insufficient under high demand), showing energy-saving and economic feasibility. Ma et al. [7] proposed a solar-assisted ASHP DHW system, providing dorm design references via modeling, experiments, and economic analysis.

In addition to solar–air-source heat pump systems, ground-source heat pumps (GSHPs) represent another efficient renewable heating option. A study by Jafarli in Azerbaijan's Khachmaz region reported a seasonal performance factor (SPF) of 4.86–5.62, achieving an annual household CO_2 reduction of 1956 kg and demonstrating the potential of shallow geothermal energy even in low-enthalpy areas [8]. Meanwhile, Zeng et al. introduced a low-carbon dispatch strategy for integrated energy systems using hydrogen

under certificate and carbon trading mechanisms, reporting substantial cost and emission reductions [9]. Wu et al. [10] proposed a ground-source absorption heat pump-based combined system for heating/cooling/DHW. Simulations showed ~20% of total condensation heat and 15% of absorption heat were recovered for DHW, with PEE of 1.516 (Beijing) and 1.163 (Shenyang)—23.6%–44.4% higher than conventional systems. Niemelä et al. [11] proposed a stepwise heating method for DHW via ground-source heat pumps, boosting energy efficiency by 45%–50% vs. traditional ones. When heating DHW from 7.5°C to 55°C, its seasonal COP reached 3.7–3.8.

For complex hybrid energy systems, multi-objective optimization combined with exergy-based analysis is essential to balance efficiency, economic viability, and environmental impact. Hajabdollahi et al. employed the NSGA-II algorithm to optimize a solar–fossil fuel cogeneration system, demonstrating its effectiveness in identifying sustainable configurations [12]. Similarly, Saleh et al. combined NSGA-II with artificial neural networks to optimize a solar–fossil fuel multi-generation system, achieving an exergy efficiency of 32.61% [13]. These advanced computational methods are increasingly important for optimizing renewable-integrated systems.

Nevertheless, current research presents several limitations. Some studies focus exclusively on heating, neglecting dynamic DHW load profiles [14], while others propose multi-source systems without climate-adaptive or capacity-optimization strategies [15]. Although notable carbon reductions have been reported—such as the 40.74% reduction achieved by Long [16]—many studies rely on regulatory standards rather than real-world operational conditions. Moreover, the trade-off between energy savings and thermal comfort during cyclic operation, widely studied in HVAC systems, remains underexplored in DHW system design [17].

To fully cover the building's domestic hot water demand, this study develops a renewable energy system combining solar thermal and air-source heat pumps (ASHP) for a medium-sized hotel in Wuhan. An immersion electric heater is incorporated into the storage tank to ensure supply during renewable shortfalls. Using the TRNSYS-TRNOPT platform, a dynamically coupled model was developed with dual objectives of improving energy efficiency and reducing emissions. The optimization, guided by the cost-benefit ratio (CBR), achieves a balance between economic feasibility and carbon reduction, offering a replicable model to support the "Dual Carbon" goals in the building sector.

2 Project Overview

2.1 Climatic Characteristics of Wuhan

Wuhan, located in the Jianghan Plain along the middle reaches of the Yangtze River, is characterized by a hot-summer and cold-winter climate. Summers are hot and humid, with average July–August temperatures of 28°C–30°C, extreme highs approaching 40°C, and relative humidity above 80%. Winters are cold and damp, with average January temperatures of 3°C–4°C, extreme lows between −5°C and −8°C, and relative humidity of 75%–85%. On an annual basis, Wuhan experiences relatively high dry-bulb temperatures, with average values of 28°C–30°C during July–August (Fig. 1).

Solar radiation in Wuhan exhibits pronounced seasonal variation (Fig. 2). Radiation intensity is high in summer and low in winter. Annual total solar radiation reaches approximately 4387 MJ/m^2 on a horizontal surface and 5766 MJ/m^2 on a tilted surface, indicating relatively abundant solar resources. The estimated solar fraction is 40%–50%.

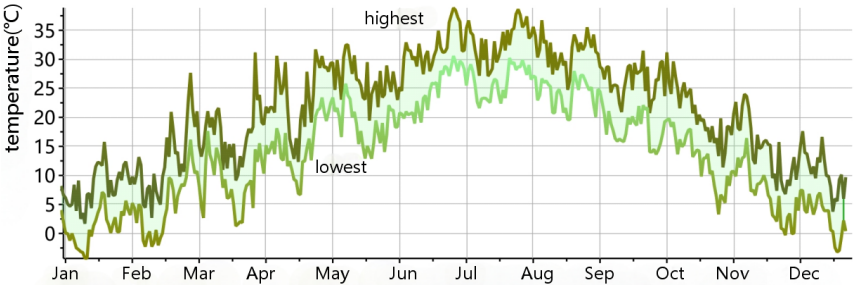

Figure 1: Annual daily dry-bulb temperature in Wuhan

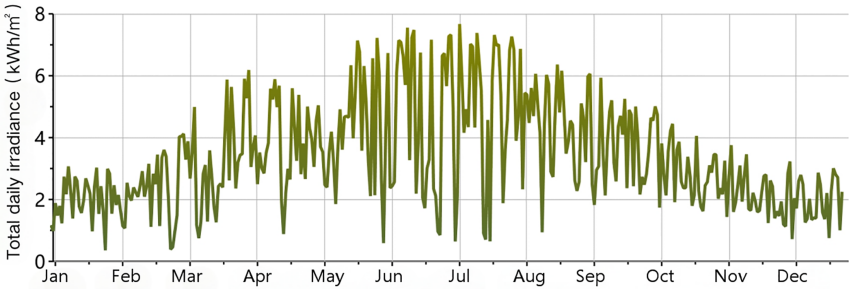

Figure 2: Seasonal variation of daily total solar radiation in Wuhan

2.2 Domestic Hot Water (DHW) Usage Pattern in the Hotel

Designing the hotel's DHW system requires careful consideration of its unique water consumption patterns, which are mainly characterized by:

- High and Stable Demand: Large hotel capacity with numerous guests and staff results in substantial DHW consumption, particularly during holidays. A continuous and stable hot water supply is required for guest rooms (washing, showering) and staff facilities.
- Concentrated Peak Periods: DHW demand peaks occur during the morning (07:00–09:00) and evening (18:00–23:00). Peak flows can reach 70%–85% of average daily demand, reflecting strong instantaneous fluctuations.

To analyze the thermal load characteristics and validate the system design, a representative four-star hotel in Wuhan was selected as a case study. The hotel has a floor area of approximately 7000 m^2, a site area of about 1000 m^2, and an available rooftop area of approximately 500 m^2. It contains 204 beds. Based on operational statistics, the annual DHW consumption is 13,716 t. This corresponds to an average daily DHW consumption quota of approximately 184 L/(bed·d). The system design hot water temperature is 60°C, requiring uninterrupted 24-h supply. Fig. 3 illustrates the daily water consumption profile, and detailed schedules are provided in Section 3.3.

Hotel DHW demand is highly dynamic, driven largely by occupancy rates that fluctuate seasonally with tourism activities. This variability leads to significant temporal changes in hot water load. To capture such dynamics, a multi-dimensional operating condition matrix was developed, incorporating occupancy levels and seasonal climate characteristics. Sixteen representative operating conditions were defined (Table 2). Occupancy discretization was parameterized as follows:

- Below 25% occupancy: Calculated uniformly at a 25% baseline to avoid statistical bias under very low load conditions. The corresponding daily DHW demand is ~9384 L/d (184 L/(bed·d) × 204 beds × 25%).

- 25%–50% occupancy: Modeled at the 50% level, giving ~18,768 L/d.
- 50%–70% occupancy: Modeled at the 70% level, giving ~26,275 L/d.
- Above 70% occupancy: Modeled at a 90% baseline to assess peak load performance, giving ~33,782 L/d.

It should be noted that the occupancy discretization model (25%, 50%, etc.) simplifies the real-world fluctuations in hotel occupancy. This approach may underestimate peak demand during holidays or special events. Furthermore, the daily demand profiles are static and do not account for intraday variability such as conference schedules or seasonal tourism surges. Future research could incorporate dynamic load models for more granular analysis. Additionally, the system design is based on a rooftop area of 500 m^2, which may limit its applicability to smaller hotels or urban buildings with space constraints.

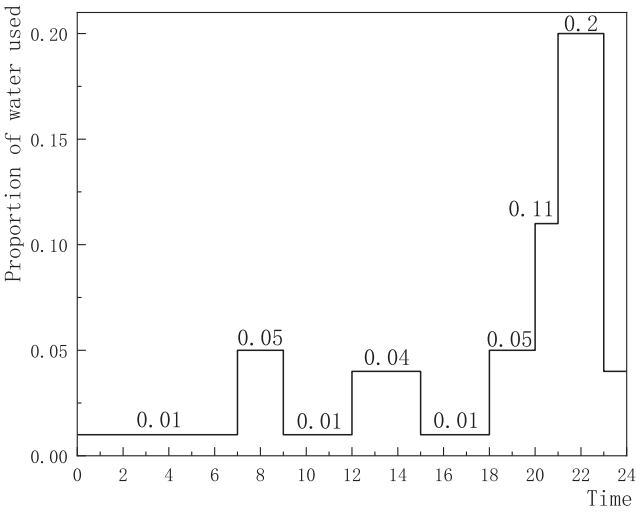

Figure 3: Daily water consumption profile

Table 2: Operating conditions matrix

Seasonal period	Dec–Feb	Mar–May	Jun–Aug	Sep–Nov
Solar radiation (kJ/m^2)	10,416.57	13,610.80	20,460.06	12,797.61
33,782 (L/d)	Condition 1-1	Condition 2-1	Condition 3-1	Condition 4-1
26,275 (L/d)	Condition 1-2	Condition 2-2	Condition 3-2	Condition 4-2
18,768 (L/d)	Condition 1-3	Condition 2-3	Condition 3-3	Condition 4-3
9384 (L/d)	Condition 1-4	Condition 2-4	Condition 3-4	Condition 4-4

3 TRNSYS Simulation and Optimization

3.1 System Architecture

The configuration of the solar–air source heat pump (SAHP) composite system for domestic hot water (DHW) supply is shown in Fig. 4. The system primarily consists of a solar collector unit, an air-source heat pump (ASHP) unit, thermal storage tanks, and auxiliary components. The solar collector unit includes collectors, a circulation pump, piping, and valves. The ASHP unit comprises the evaporator, compressor, condenser, expansion valve, a circulation pump, and related piping and valves. The auxiliary electric heating unit adopts an immersed axial configuration installed within 20%–80% of the tank's effective volume to minimize top/bottom flow disturbance. It features flange-sealed connections (pressure rating ≥ 0.6 MPa) and

is integrated with temperature sensors, enabling gradient heating control to reduce unnecessary dissipation of high-grade electrical energy.

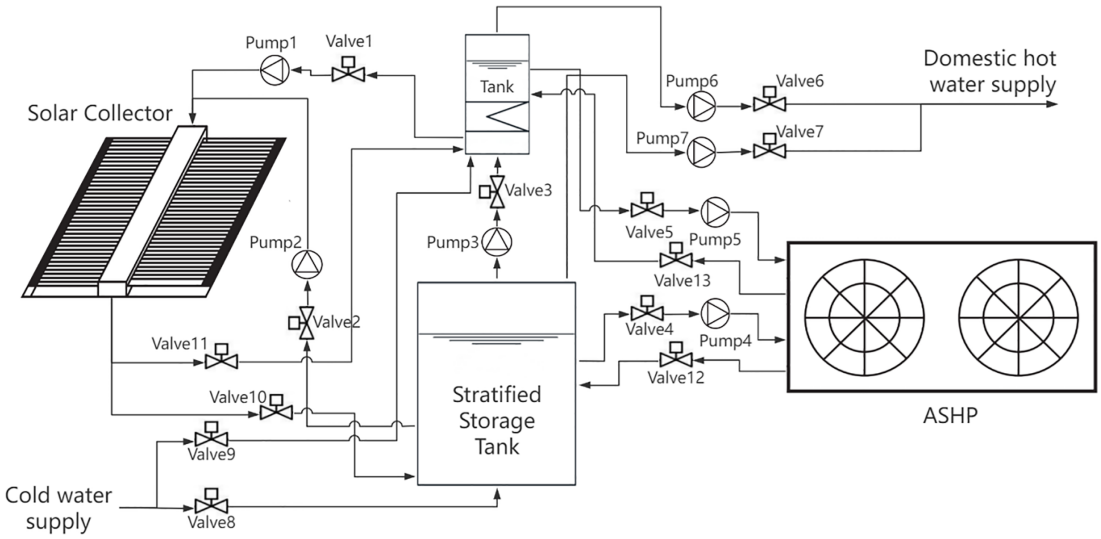

Figure 4: Schematic diagram of the solar-air source heat pump composite system

The SAHP system operates under four main modes:

- Solar-Priority Mode (High Insolation, e.g., Summer): When solar irradiance is sufficient, solar collectors are prioritized to meet most of the DHW demand. Once the heating tank reaches the setpoint, excess heat is stored in the storage tank. Overheat protection (cut-off at 95°C) prevents boiling.
- ASHP-Priority Mode (Low/No Solar, e.g., Winter): When irradiance is insufficient or storage tank temperature falls below 55°C, the ASHP is activated to heat the tank to 60°C before deactivation.
- Solar-ASHP Hybrid Mode: Under unstable or intermittent solar radiation, the ASHP supplements solar heating to ensure stable supply.
- Auxiliary Electric Heating Mode: Following a "renewables-first, smart backup" strategy, the electric heater activates when collector outlet temperature < 52°C and condenser $\Delta T > 8$°C. The controller modulates heater power to maintain tank temperature at 60 ± 2°C.

3.2 Mathematical Models of Key Components

3.2.1 Solar Collector

A nano-coated evacuated tube collector with a maximum photothermal conversion efficiency of 91.7% was adopted. It is important to note that the claimed photothermal efficiency of 91.7% for the nano-coated tubes is based on literature [18] and lacks independent experimental verification under Wuhan's specific climate conditions, particularly regarding long-term durability. The instantaneous efficiency is calculated as [19]:

$$\eta_I = \eta_0 - a_1 \frac{(T_i - T_a)}{G} - a_2 G \left(\frac{T_i - T_a}{G} \right)^2 \quad (1)$$

where: η_0—Intercept efficiency (0.8 in this study); a_1—First-order heat loss coefficient (0.015 W/(m^2·K)); a_2—Second-order heat loss coefficient (0.01 W/(m^2·K)^2); T_i—Inlet water temperature (K); T_a—Ambient air temperature (K); G—Instantaneous solar irradiance (W/m^2).

3.2.2 Air Source Heat Pump (ASHP)

A low-temperature variable-frequency vapor-injection ASHP is used. To account for performance degradation caused by frosting, a correction factor (K_1 = 0.9) is introduced. The frosting correction factor K_1 = 0.9 is an empirical value derived from general operating conditions. Its accuracy under Wuhan's high-humidity winter conditions requires further empirical validation. Heating capacity is expressed as [20]:

$$q = Q/K_1 \tag{2}$$

where: Q—Actual heating capacity (kW).

Additional correction coefficients for heating capacity and power in cold climates are embedded via external data (Fig. 5).

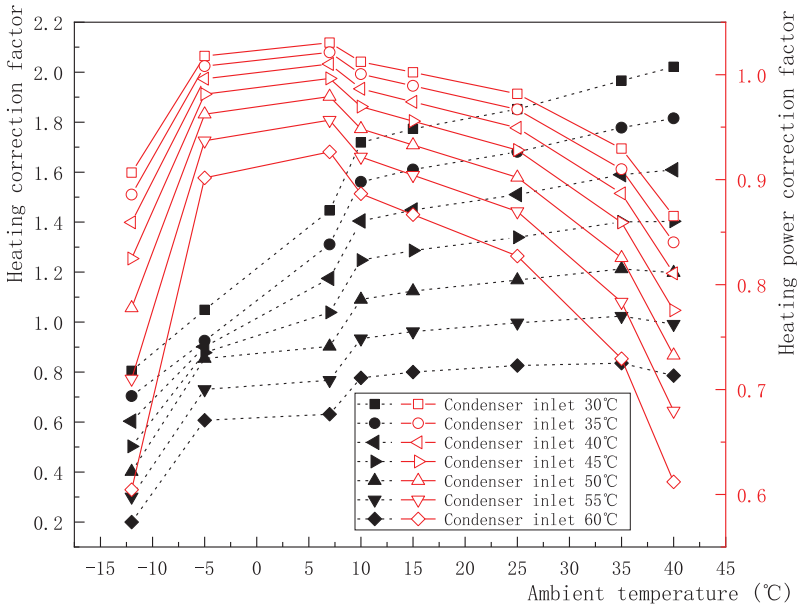

Figure 5: Heating capacity and power correction coefficients for ASHP

3.2.3 Thermal Storage Tank

A stratified storage tank is employed to improve thermal efficiency. The energy balance is given by [21]:

$$\left(V_s \cdot C_{p,w} \cdot \rho_w\right) \frac{dt}{d\tau} = \left(Q_u\right)_s - Q_r - \left(U \cdot A\right)_s \left(t_s - t_a\right) \tag{3}$$

where: V_s—Circulating water volume during collection (m^3); $(U{\cdot}A)_s$—Tank heat loss coefficient (W/°C); Q_r—Daily thermal energy input (J/d); $C_{p,w}$—Water specific heat (4180 J/(kg·°C)); ρ_w—Water density (990 kg/m^3).

The calibrated heat loss coefficient may vary over the system's lifespan due to aging of insulation materials or lack of maintenance. This long-term degradation effect is not accounted for in the present study.

3.2.4 Pump

The energy consumption of a circulation pump is primarily determined by its flow rate, head, and operating efficiency. The instantaneous electrical power consumption of the pump, P (kW), is calculated

using the following formula:

$$P = \frac{\rho g H V}{1000 \eta_p \eta_m} \tag{4}$$

where: ρ—Density of the fluid (kg/m^3); g—Gravitational acceleration (m/s^2); H—Total dynamic head required by the pump under actual operating conditions (m); V—Volumetric flow rate of the fluid (m^3/s); η_p—Isentropic efficiency of the pump itself; η_m—Efficiency of the drive motor.

3.3 TRNSYS Model Development

The TRNSYS simulation model of the SAHP system is shown in Fig. 6. The main components and functions are listed in Table 3.

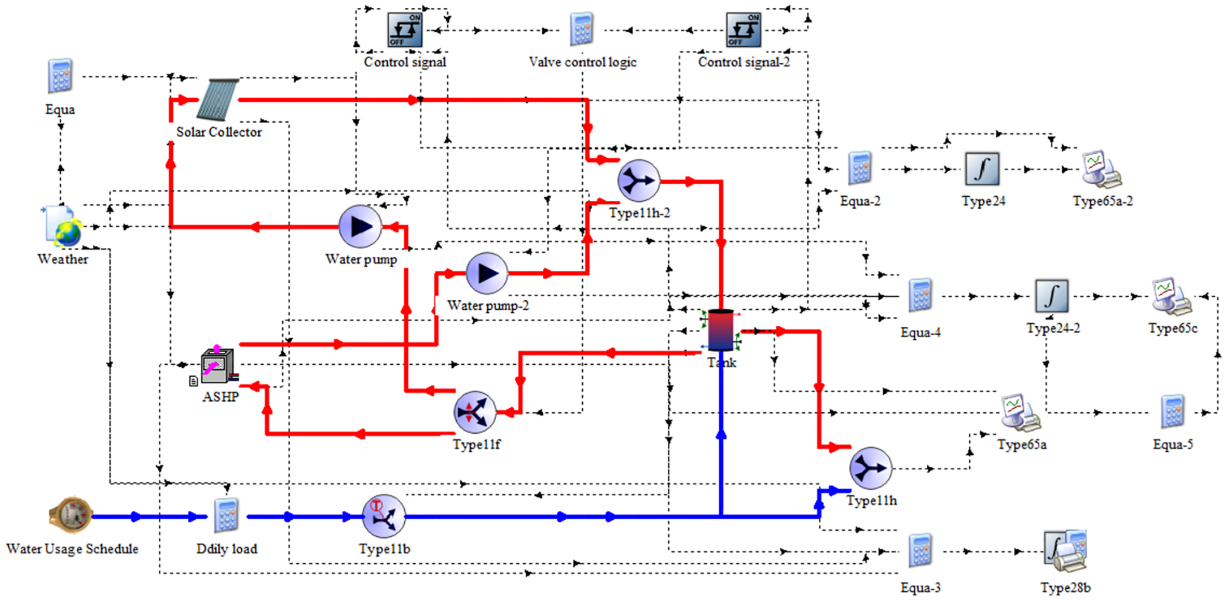

Figure 6: TRNSYS simulation model architecture

Table 3: Operating conditions matrix

Component type	Component name	Quantity	Functionality description
Type15-2	Meteorological data	1	Reads Wuhan climate data from Meteonorm
Type14b	Water usage schedule	1	Simulates hourly DHW demand
Type71	Solar collector	1	Models collector with area, azimuth, tilt angle. Initial area calculated per Ref. [22]
Type4c	Stratified storage tank	2	Models tank (23 parameters, 7 inputs)
Type491	ASHP unit	1	Models ASHP with capacity/power inputs
Type114	Circulation pump	2	Models flow, head, and power

(Continued)

Table 3 (continued)

Component type	Component name	Quantity	Functionality description
Type2b	Differential controller	2	Implements start/stop control
Equa	Equation calculator	6	Performs unit conversion and logic operations

3.4 Model Validation

To verify reliability, on-site data from the hotel's existing gas boiler system were collected (Nov 2023–Jan 2024). Boundary conditions (supply temperature, flow) were applied for reverse calibration. By adjusting collector efficiency and tank heat loss coefficients, simulation–measurement deviation was controlled within 8% (Fig. 7). This meets ASHRAE Guideline 14-2014 requirements (<10%), confirming the model's validity. It should be emphasized that the model validation was conducted only from November to January. Consequently, the system's performance during summer conditions, such as potential collector overheating, lacks empirical verification and should be investigated in future work.

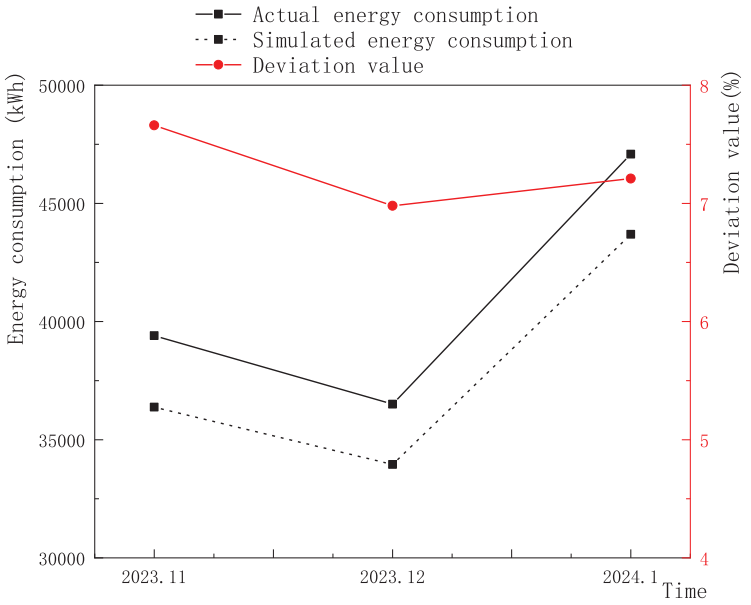

Figure 7: Comparison of actual and simulated energy consumption

3.5 TRNOPT Optimization Framework

The setting of optimization variables and objective functions is premised on achieving full-capacity supply. Within the TRNOPT platform, with the constraint that the system must meet the maximum design hot water load under all-weather and all-season conditions, parameters such as collector area, tilt angle, azimuth angle, heat pump heating capacity, and tank volume were co-optimized. The optimization objective function CBR (Cost-Benefit Ratio) essentially reflects the incremental cost per unit of energy saved over the system's entire life cycle while ensuring full-capacity supply, thereby achieving a unity of economy and functionality.

3.5.1 Optimization Parameters

Based on previous research, five parameters were selected: solar collector area, collector tilt angle, collector azimuth angle, ASHP rated heating capacity, and thermal storage tank volume. Initial values for each operating condition are provided in Table 4.

Table 4: Initial values of optimization parameters

Condition	Collector area (m^2)	ASHP rated capacity (kW)	Tank Vol (m^3)	Tilt angle (°)	Azimuth angle (°)	Condition	Collector area (m^2)	ASHP rated capacity (kW)	Tank Vol (m^3)	Tilt angle (°)	Azimuth angle (°)
Cond1-1	500	142	50	45	0	Cond3-1	340	103	34	45	0
Cond1-2	500	110	50	45	0	Cond3-2	264	80	26.4	45	0
Cond1-3	500	78	50	45	0	Cond3-3	189	57	18.9	45	0
Cond1-4	255	40	25.5	45	0	Cond3-4	95	29	9.5	45	0
Cond2-1	500	116	50	45	0	Cond4-1	500	116	50	45	0
Cond2-2	447	90	44.7	45	0	Cond4-2	475	90	47.5	45	0
Cond2-3	319	64	31.9	45	0	Cond4-3	340	64	34	45	0
Cond2-4	160	32	16	45	0	Cond4-4	170	32	17	45	0

Optimization was conducted under the constraint that the system must meet maximum DHW load across all conditions. Five variables were co-optimized (Table 5).

Table 5: Ranges and step sizes for optimization variables

Variable	Minimum	Maximum	Step size
Collector area (m^2)	50	500	5
Collector slope angle (°)	20	80	1
Collector azimuth angle (°)	−15	15	1
ASHP rated capacity (kW)	20	200	1
Volume-to-area ratio (m^3/m^2)	0.02	0.5	0.02

3.5.2 Objective Function

The Cost-Benefit Ratio (CBR) was used as the objective function, defined as the incremental cost per unit of energy saved over the system lifetime [23].

$$CBR = \frac{L}{N \times Q} \tag{5}$$

where: L—Incremental investment (CNY); N—System lifespan (15 years); Q—Annual energy savings (kWh).

The initial investment cost model is defined as:

$$L_0 = A_0 * C_1 + V_0 * C_2 + Q_0 * C_3 + L_1 \tag{6}$$

where: L_0—Collector area (m^2); C_1—Unit area investment cost of the collector (500 CNY/m^2); V_0—Storage tank volume (m^3); C_2—Unit volume investment cost of the storage tank (1100 CNY/m^3); C_3—Unit heating capacity investment cost of the heat pump (600 CNY/kW); L_1—Additional costs (15,000 CNY).

3.5.3 Optimization Model

The TRNOPT framework (Fig. 8) employed the Hooke–Jeeves algorithm for multi-variable optimization. The Hooke–Jeeves algorithm operates through an iterative sequence of exploratory and pattern moves. Beginning from an initial point, exploratory moves probe along coordinate axes with a specified step size to identify a point with improved objective function value. If successful, a pattern move is executed in the direction from the previous to the new base point, accelerating the search. The success of this pattern direction is then verified by a new exploratory move. If no improvement is found after a pattern move, the algorithm reverts to the previous base point. The step size is reduced if exploratory moves fail in all directions, refining the search resolution. The process continues until the step size falls below a predefined tolerance. This gradient-free approach is particularly suitable for optimizing computationally expensive simulations, such as those encountered in engineering system design. Compared with Newton's method or complex metaheuristics (e.g., genetic algorithms, ant colony), Hooke–Jeeves demonstrated superior convergence speed and stability [24]. While the Hooke-Jeeves algorithm was selected for its rapid convergence and stability in this application, it is recognized that, as a direct search method, it may converge to local minima. A comparative analysis with global metaheuristic algorithms (e.g., Genetic Algorithms) was beyond the scope of this study but represents a valuable direction for future research.

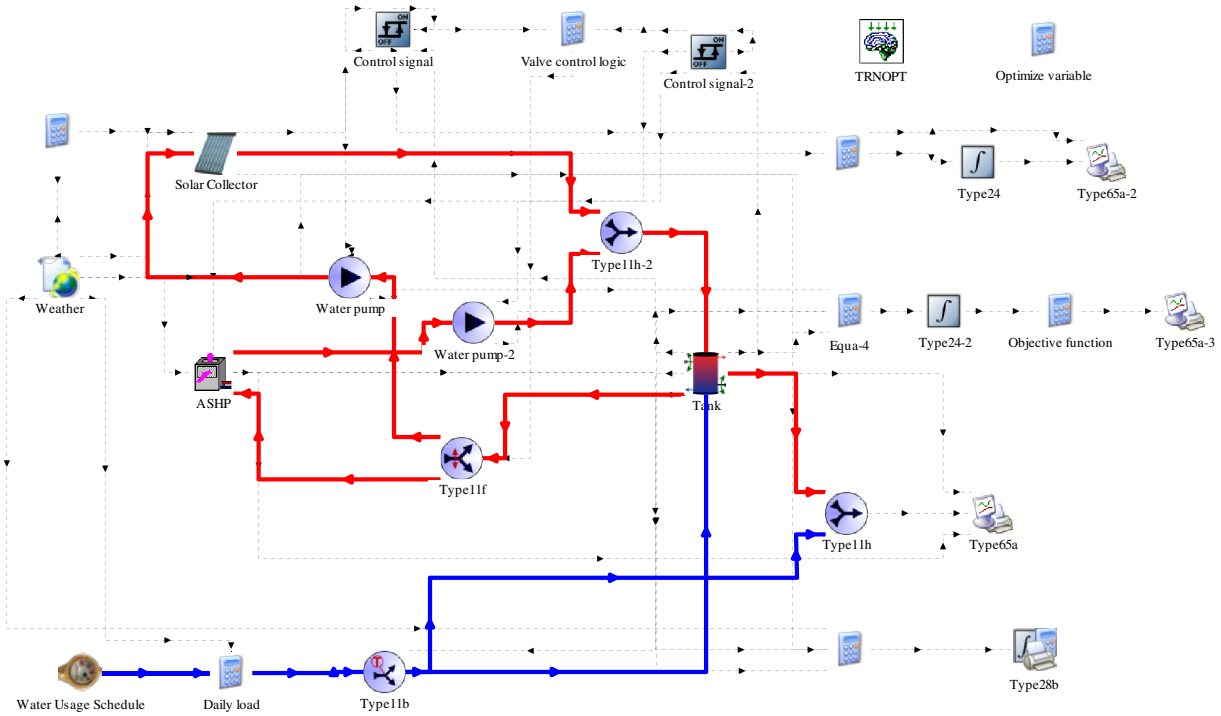

Figure 8: TRNOPT optimization model for SAHP DHW system

4 Results and Discussion

4.1 Model Reliability Verification

To verify the reliability of the optimization model, 500 iterations were conducted using the Hooke–Jeeves algorithm within the GenOpt platform, with a convergence precision of 5%. The variation trend of the objective function is shown in Fig. 9.

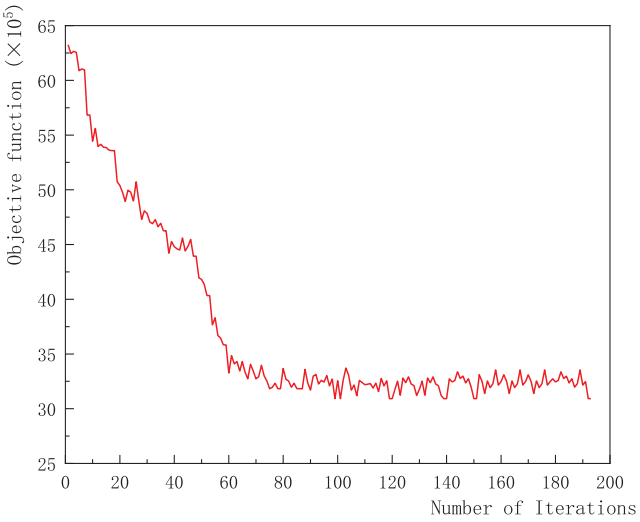

Figure 9: Trend of objective function variation

As illustrated, the objective function stabilized after approximately 60 iterations. Within the optimized parameter range, output indicators exhibited only minor fluctuations, confirming controllability. The algorithm progressively approached and stabilized at the optimal solution, demonstrating both convergence and robustness. These results indicate that the system can maintain stability under long-term operation and varying initial conditions.

4.2 Optimization Outcomes

Optimization simulations were carried out for all operating conditions. The minimized cost–benefit ratio (CBR) indicates lower cost per unit of benefit and higher resource utilization efficiency, representing the most balanced solution among energy savings, environmental performance, and cost. Fig. 10 compares solar collector area and ASHP rated capacity before and after optimization, while Fig. 11 presents the final optimized values.

The results show that the optimized solar collector area increased significantly. The maximum increase (65%) occurred during December–February, while average increases were 17.3% (Mar–May), 11.8% (Jun–Aug), and 16.7% (Sep–Nov). This trend reflects TRNOPT's proactive capacity-expansion strategy, which enhances the solar fraction by capturing additional irradiation to reduce ASHP consumption.

In contrast, ASHP capacity optimization displayed strong seasonal divergence. During December–February, ASHP capacity increased markedly (14%–92.5%) due to limited solar irradiation (15% of annual sunshine hours), requiring the ASHP to shoulder most of the heating load. From March to November, ASHP capacity remained stable or slightly decreased, owing to higher solar fractions under stronger irradiation. Nevertheless, in June–August, despite abundant radiation, ASHP capacity exceeded that of March–May due to high demand combined with the persistent plum rain season.

Fig. 11 also shows stable collector tilt and azimuth angles across all conditions, with tilt varying between 32°–47° and azimuth between −2°–8°. This low sensitivity highlights the system's adaptability to geographical latitude. In contrast, tank volume optimization revealed a dynamic seasonal adaptation:

- Dec–Feb (low insolation): Storage volume per collector area was reduced to minimize heat loss and improve efficiency.

- Mar–May & Sep–Nov (transitional seasons): Tank volume increased by 20%–100% per unit area to enhance storage and buffer load fluctuations.
- Jun–Aug (peak insolation): Tank volume more than doubled, enabling surplus heat storage and cross-period transfer.

This coordinated optimization establishes a responsive mechanism to adapt to both climatic variability and load dynamics. Collector angles ensured stable capture efficiency, while tank capacity enabled energy time-shifting, highlighting the essence of dynamic system optimization.

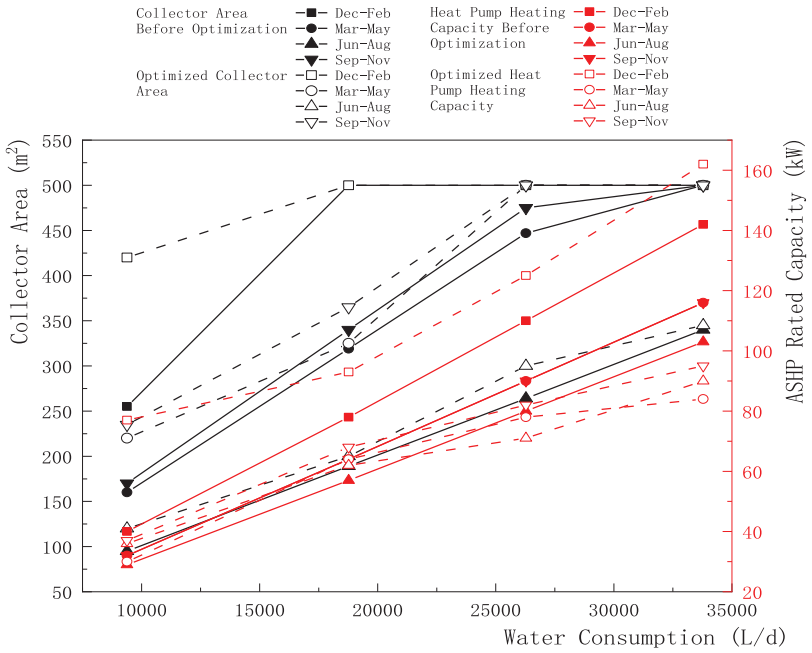

Figure 10: Comparison of collector area and heat pump capacity before and after optimization

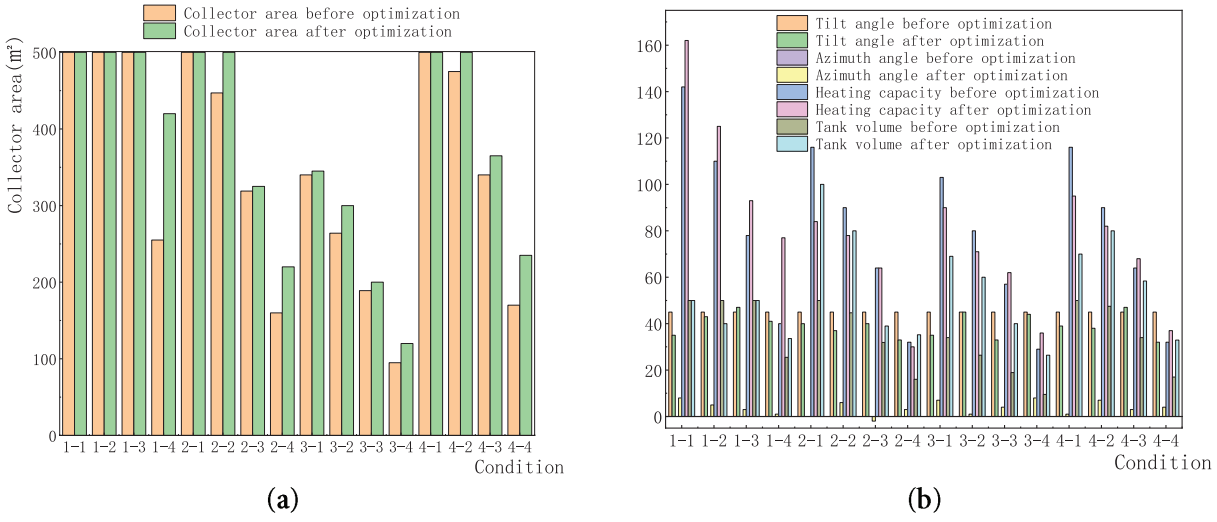

Figure 11: Comparison of optimization variables before and after under 16 conditions. (**a**) Optimization of collector area before and after; (**b**) Four variables before and after optimization

4.3 Comprehensive System Evaluation

The optimized SAHP system relies solely on electricity for operation, without direct CO_2 emissions. Carbon emissions were calculated using an emission factor of 0.4364 $kgCO_2$/kWh, based on the Provincial Greenhouse Gas Inventory Guide (Ministry of Ecology and Environment, 2022), ensuring regional applicability.

To compare performance, four optimized cases (1-1, 2-1, 3-1, 4-1) representing actual hotel demand (~37,578 L/d) were selected against the traditional gas boiler benchmark (annual natural gas consumption: 45,322 m^3). The gas-to-standard-coal conversion factor of 1.2143 kgce/m^3 was applied.

Based on the results presented in Table 6, it can be concluded that all optimized cases provided full-capacity supply while significantly reducing energy consumption and emissions. Case 1-1 performed best, achieving 60.8% energy savings and an annual carbon reduction of 132.8 t. This was mainly due to the algorithm's expansion of collector area (+65%) and dynamic tank storage optimization, reducing reliance on ASHP.

Table 6: Comparison of comprehensive indicators

	Gas Boiler	Cond 1-1	Cond 2-1	Cond 3-1	Cond 4-1
Energy consumption (kWh)	453,220	179,305.2	200,971.2	328,893	196,070.1
Converted standard coal (kgce)	59,168.4	23,212.1	25,874.8	41,596.4	25,272.5
System carbon emissions (kg)	219,761.3	86,943.1	97,448.7	159,476.6	95,072.2
Initial investment (CNY)	–	417,200	425,400	317,400	399,000
Operating expenses (CNY)	–	100,052.3	112,141.9	183,522.3	109,407.1
Energy saving rate	–	60.8%	56.3%	29.7%	57.3%

Economic evaluation was further conducted by calculating the investment payback period (PP). As shown in Table 7, although Case 1-1 required higher upfront investment, its superior energy savings reduced the PP to only 4.1 years, below the common industry benchmark of 6–8 years.

Table 7: Comparison of economic indicators

Condition	Initial investment × 10^4 (CNY)	Annual operating expenses × 10^4 (CNY)	Annual energy saving benefits × 10^4 (CNY)	Payback period (y)
1-1	41.7	10.0	15.2	4.1
3-1	31.7	18.4	8.9	6.8

Overall, the coordinated optimization of multi-equipment parameters and dynamic operational strategies effectively overcomes the limitations of conventional systems under extreme conditions, ensuring safe, stable, and continuous full-capacity DHW supply. Cases 1-1 and 4-1 are most suitable under an environment-prioritized strategy, with energy savings >57% and significant carbon reductions. For investment-focused strategies, Case 3-1 offers a lower initial cost, while Case 1-1 balances investment with long-term efficiency.

This study has several limitations that should be considered. The economic analysis assumes stable electricity prices and fixed unit costs for components; future price volatility or bulk purchase discounts could alter the economic outcomes. The carbon emission calculation employs a static grid emission factor,

which does not account for the ongoing decarbonization of the regional power grid over the system's 15-year lifespan. Moreover, this work focuses on operational carbon emissions, omitting the embodied carbon from the manufacturing and installation of the solar and ASHP components. Finally, the analysis prioritizes energy savings and economic performance, and does not evaluate guest comfort aspects, such as temperature stability during ASHP defrost cycles.

In summary, the proposed optimization framework fundamentally restructures the energy mix of hotel hot water systems, achieving multidimensional improvements in energy efficiency, carbon reduction, and economic performance. This provides a practical technical pathway and decision-making basis for the low-carbon transition of hotel DHW systems.

5 Conclusion

Focusing on the demand for full-load domestic hot water supply in hotels, this study developed an integrated system that dynamically couples solar thermal energy with an air-source heat pump (ASHP). Multi-condition optimization and comprehensive performance evaluation were carried out using the TRNSYS-TRNOPT platform. The main conclusions are as follows:

(1) The system achieves a balance between full-load supply and high energy efficiency: Through optimization under 16 multidimensional operating conditions, the system consistently meets the hotel's round-the-clock hot water demand across different seasons and occupancy rates. The optimal case (Case 1-1) achieves an energy saving rate of 60.8% and an annual carbon reduction of 132.8 t, validating the technical feasibility of completely replacing conventional gas boilers with a renewable energy system.

(2) A climate-load adaptive mechanism represents a key breakthrough: The optimization algorithm dynamically adjusts equipment parameters in response to external variations. By introducing the joint optimization indicator of "storage volume per unit collector area", a precise match between thermal storage capacity and climatic conditions is achieved. The tank volume is increased by threefold in summer to store surplus heat, while in winter, the collector area and heat pump capacity are significantly raised (+65% and +92.5%, respectively) to compensate for insufficient solar energy.

(3) The system demonstrates favorable economic performance: The optimal case (Case 1-1) yields a payback period of 4.1 years, which is lower than common industry benchmarks, highlighting the economic attractiveness of this technical pathway.

This study provides a design reference for the low-carbon renovation of hotels in hot-summer and cold-winter regions. Future research should focus on integrating phase-change materials for thermal storage or photovoltaic (PV) panels to mitigate performance degradation during prolonged rainy periods and to further enhance renewable energy utilization. Additionally, the impact of system operation on guest comfort, particularly during ASHP defrost cycles, warrants detailed investigation.

Acknowledgement: Not applicable.

Funding Statement: The authors received no specific funding for this study.

Author Contributions: The authors confirm contribution to the paper as follows: study conception and design: Zhongyi Yu; data collection: Chunzhi Zhang; analysis and interpretation of results: Lanyue Liu; supervision: Chunzhi Zhang, Zhongyi Yu; draft manuscript preparation: Lanyue Liu; draft manuscript review and editing: Lanyue Liu, Chunzhi Zhang, Zhongyi Yu. All authors reviewed the results and approved the final version of the manuscript.

Availability of Data and Materials: Data available on request from the authors.

Ethics Approval: Not applicable.

Conflicts of Interest: The authors declare no conflicts of interest to report regarding the present study.

References

1. Yu L, Wu S, Jiang L, Ding B, Shi X. Do more efficient buildings lead to lower household energy consumption for cooling? Evidence from Guangzhou, China. Energy Policy. 2022;168:113119. doi:10.1016/j.enpol.2022.113119.
2. Li XJ. Comprehensive comparative analysis of hotel hot water heat source selection incorporating carbon reduction assessment. In: Proceedings of 16th Building Water Supply and Drainage Conference; 2024 Oct 24; Guangzhou, China.
3. International Energy Agency. Transition to sustainable buildings: strategies and opportunities to 2050. Paris, France: IEA Publications; 2013. doi:10.1787/9789264202955-en.
4. Wang F, Liu Y, Zhang J. A review of solar-assisted heat pump systems for building applications. Energy Build. 2023;285:112943.
5. Bhadra S, Mwesigye A. Influence of control strategy on the energetic performance of an air source heat pump coupled with a solar air collector for domestic hot water in a cold climate. Renew Energy. 2025;244:122682. doi:10.1016/j.renene.2025.122682.
6. Ma Y, Xi J, Cai J, Gu Z. TRNSYS simulation study of the operational energy characteristics of a hot water supply system for the integrated design of solar coupled air source heat pumps. Chemosphere. 2023;338:139453. doi:10.1016/j.chemosphere.2023.139453.
7. Ma S, Lu S, Ma D, Li C, Liu C, Wu L, et al. Investigation on the thermal performance and economy of a solar assisted air source heat pump domestic hot water system. Appl Therm Eng. 2023;232:121007. doi:10.1016/j.applthermaleng.2023.121007.
8. Jafarli O. Analysis of the use of geothermal energy for heating in Azerbaijan. Energy Eng. 2025;122(9):3595–608. doi:10.32604/ee.2025.067982.
9. Zeng A, Wang Z, Wang J, Hao S, Wang M. Low-carbon economic dispatch strategy for integrated energy systems with blue and green hydrogen coordination under GHCT and CET mechanisms. Energy Eng. 2025;122(9):3793–816. doi:10.32604/ee.2025.069410.
10. Wu W, You T, Wang B, Shi W, Li X. Simulation of a combined heating, cooling and domestic hot water system based on ground source absorption heat pump. Appl Energy. 2014;126:113–22. doi:10.1016/j.apenergy.2014.04.006.
11. Niemelä T, Manner M, Laitinen A, Sivula TM, Jokisalo J, Kosonen R. Computational and experimental performance analysis of a novel method for heating of domestic hot water with a ground source heat pump system. Energy Build. 2018;161:22–40. doi:10.1016/j.enbuild.2017.12.017.
12. Hajabdollahi H, Saleh A, Yadollahi NK. Multi-objective optimization of a solar-assisted cogeneration system in hot climate: an exergoeconomic and exergoenvironmental assessment. Therm Sci Eng Prog. 2025;62:103656. doi:10.1016/j.tsep.2025.103656.
13. Saleh A, Ghamari V, Hajabdollahi H. Efficient design of solar-fossil fuel multi-generation system using artificial intelligence. Appl Therm Eng. 2025;278:127231. doi:10.1016/j.applthermaleng.2025.127231.
14. Razavi SH, Ahmadi R, Zahedi A. Modeling, simulation and dynamic control of solar assisted ground source heat pump to provide heating load and DHW. Appl Therm Eng. 2018;129:127–44. doi:10.1016/j.applthermaleng.2017.10.003.
15. Li N, Li KY, Wang J. Study on the application of multi-energy complementary living hotwater heating system available for hotel energy conservation. Electr Saf Technol. 2024;26(2):32–6. (In Chinese). doi:10.3969/j.issn.1008-6226.2024.02.010.
16. Long YQ. Design practice of low temperature air source heat pump and solar powered hot water supply system in hospital. Shanxi Archit. 2024;50(18):104–8,135. (In Chinese). doi:10.13719/j.cnki.1009-6825.2024.18.025.
17. Agharid AP, Permana I, Chang L, Luo YH, Wang F. Impact of duty cycling HVAC systems on thermal comfort, energy consumption, and operational costs. Energy Eng. 2025;122(9):3839–66. doi:10.32604/ee.2025.068586.

18. Sathish T. Thermal performance assessment by cerium oxide nano-enhanced coating on evacuated tube solar collector absorber tubes. Results Eng. 2025;25:104396. doi:10.1016/j.rineng.2025.104396.
19. Li C. Performance study on domestic hot water supply system with solar-air source heat pump composite heat source [master's thesis]. Tianjin, China: Tianjin University; 2020.
20. GB 19577-2024. State administration for market regulation, standardization administration of China. In: Minimum allowable values of energy efficiency and energy efficiency grades for heat pumps and chillers. Beijing, China: China Standards Press; 2024.
21. Tang YF. Regional and load adaptability research of solar-air source heat pump heating systems based on TRNSYS [master's thesis]. Guangzhou, China: Guangdong University of Technology; 2022.
22. GB 50364-2018. Technical standard for solar water heating systems of civil buildings. Beijing, China: Chinese National Standards; 2018.
23. GB/T 50801-2013. Evaluation standard for renewable energy building applications. Beijing, China: Chinese National Standards; 2013.
24. Yuan PL, Huang FY, Gao ST, Duanmu L, Wang ZS. Study on the impact of different energy usage modes on solar-air source heat pump complementary heating system. Dist Heat. 2024;4:23–31. (In Chinese). doi:10.16641/j.cnki.cn11-3241/tk.2024.04.004.